Quantitative photoacoustic estimates of intervascular blood oxygenation differences using linear unmixing

Quantitative photoacoustic estimates of intervascular blood oxygenation differences using linear unmixing

C Bench and B Cox

Department of Medical Physics and Biomedical Engineering, University College London, London, UK. WC1E 6BT

E-mail: ciaran.bench.17@ucl.ac.uk

Abstract. The linear unmixing technique is an appealing method for estimating blood oxygen saturation (sO_2) from multiwavelength photoacoustic tomography images, as estimates can be acquired with a straightforward matrix inversion. However, the technique can only rarely provide accurate estimates *in vivo*, as it requires that the light fluence at the voxels of interest is constant with wavelength. One way to extend the set of cases where accurate information related to sO_2 can be acquired with the technique is by taking the difference in sO_2 estimates between vessels. Assuming images are perfectly reconstructed, the intervascular difference in sO_2 estimates is accurate if the error in the estimates due to the wavelength dependence of the fluence is identical for both. An *in silico* study was performed to uncover what kinds of conditions may give rise to accurate sO_2 differences for a vessel pair. Basic criteria were formulated in simple tissue models consisting of a pair of vessels immersed in two-layer skin models. To assess whether these criteria might still be valid in more realistic imaging scenarios, the sO_2 difference was estimated for vessels in more complex tissue models.

1. Introduction

Photoacoustic (PA) tomography is a hybrid modality that can produce images of tissue with the specificity of optical techniques and the high spatial resolution of ultrasound [1]. The source of contrast in a PA image is the optical absorption of the tissue. Therefore, PA images of tissue contain information about the concentrations of haemoglobin (Hb) and oxyhaemoglobin (HbO_2) present and can in principle be used to generate images of blood oxygenation [2]. However, in practice this is not straightforward. The amplitude of a noise and artefact free PA image of the initial acoustic pressure distribution, p_0, can be described by

$$p_0(\mathbf{x}, \lambda) = \Gamma(\mathbf{x})\Phi(\mathbf{x}, \lambda; \mu_a, \mu_s, g)\mu_a(\mathbf{x}, \lambda), \tag{1}$$

where $\mathbf{x}$ is position within the sample, λ is the optical wavelength, Γ is the PA efficiency (assumed here to be wavelength-independent), and Φ is the optical fluence distribution, which depends on the optical absorption and scattering coefficients, μ_a and μ_s, as well as the optical anisotropy factor g. More specifically, for a voxel containing blood (assumed to contain no significant optical absorbers other than Hb and HbO_2) the photoacoustic amplitude spectrum $p_0(\lambda)$ can be related to the concentrations of Hb and HbO_2 as

$$\begin{bmatrix} p_0(\lambda_1) \\ \vdots \\ p_0(\lambda_N) \end{bmatrix} = \Gamma \begin{bmatrix} \Phi(\lambda_1) & \dots & 0 \\ \vdots & \ddots & \vdots \\ 0 & \dots & \Phi(\lambda_N) \end{bmatrix} \begin{bmatrix} \alpha_{Hb}(\lambda_1) & \alpha_{HbO_2}(\lambda_1) \\ \alpha_{Hb}(\lambda_2) & \alpha_{HbO_2}(\lambda_2) \\ \vdots & \vdots \\ \alpha_{Hb}(\lambda_N) & \alpha_{HbO_2}(\lambda_N) \end{bmatrix} \begin{bmatrix} C_{Hb} \\ C_{HbO_2}, \end{bmatrix} \tag{2}$$

where $\alpha_{Hb}(\lambda)$ and $\alpha_{HbO_2}(\lambda)$ are the molar absorption coefficient spectra of Hb and HbO_2 respectively, and N is the number of wavelengths. The blood oxygenation saturation, sO_2, is given by the ratio

$$sO_2 = \frac{C_{HbO_2}}{C_{HbO_2} + C_{Hb}}. \tag{3}$$

It is clear from Eqs. (1)-(2) that, in general, knowledge of the fluence spectrum, $\Phi(\lambda)$, is required if the PA spectrum in a voxel is to be used to estimate the sO_2. This fluence spectrum depends on the (unknown) optical properties throughout the tissue. The resulting difference between the absorption spectrum, $\mu_a(\lambda)$, and the PA spectrum, $p_0(\lambda)$, is known as *spectral colouring* [2].

In some cases the fluence can be estimated using an adjunct modality [3], but more commonly it is estimated with the help of a model. For instance, iterative model-based minimisation approaches have been used to recover phantom optical properties from PA data [4–7], but this is computationally intensive, and in practice some aspects of the data acquisition pathway are not fully characterised and so sufficiently accurate models of image generation are challenging to formulate [8]. To avoid this, techniques based on data-driven models, such as Deep Learning, have been used to output images of sO_2 from PA images of phantoms and simulated images of tissue models [9–15]. However, this approach requires a large training set of $(p_0(x, \lambda), \text{true } sO_2(x))$ pairs, which are difficult to acquire *in vivo*, and if simulated training data is used the same model mismatch problem as above returns.

There is still currently a need, therefore, for straightforward techniques that can be used *in vivo* to estimate sO_2 from PA images. Xia et al. [16] used the assumption that the fluence remains unchanged for two different oxygenation states to estimate blood sO_2, but this is unlikely to be the case *in vivo* as the oxygenation of neighbouring capillaries change in tandem with the target vessel and the optical properties of the tissue, and thus the fluence will consequently vary. Another approach has been to use 1D analytical fluence models (e.g. Beer-Lambert Law) to estimate the wavelength-dependence of the fluence, either by fitting to the data or using values reported in the literature [17–22]. When considering the practicality of a technique, the virtues of robustness, simplicity, and speed must be considered alongside accuracy. It is of great practical interest, therefore, to know if there are cases or scenarios where sO_2 can be directly estimated from the PA spectrum using *linear unmixing* without having to estimate the fluence at all. This involves finding situations in which the fluence is approximately independent of the wavelength.

1.1. Spectroscopic Linear Unmixing

When the fluence is wavelength independent, the matrix containing the fluences in Eq. (2) is proportional to the identity matrix (i.e. the PA spectrum is the optical absorption spectrum scaled by the wavelength independent constant $\Gamma\Phi$), and Eq. (2) can be inverted to recover the relative chromophore concentrations as follows:

$$\begin{bmatrix} C_{Hb} \\ C_{HbO_2} \end{bmatrix} \propto \begin{bmatrix} \alpha_{Hb}(\lambda_1) & \alpha_{HbO_2}(\lambda_1) \\ \alpha_{Hb}(\lambda_2) & \alpha_{HbO_2}(\lambda_2) \\ \vdots & \vdots \\ \alpha_{Hb}(\lambda_N) & \alpha_{HbO_2}(\lambda_N) \end{bmatrix}^{\dagger} \begin{bmatrix} p_0(\lambda_1) \\ \vdots \\ p_0(\lambda_N) \end{bmatrix}, \tag{4}$$

where the † denotes the pseudoinverse. These relative concentrations can then be used to estimate absolute sO_2 using Eq. (3). When is this useful? The fluence can be sometimes be considered independent of wavelength when measuring superficial vessels [23–26]. Also, careful selection of the optical wavelengths can also help reduce the wavelength dependence of the fluence distribution [27]. However, choosing the ideal wavelengths without prior knowledge of tissue's optical properties (and simultaneously ensuring that at these wavelengths the matrix of molar absorption coefficients is well-conditioned) is highly challenging.

1.2. Paper Outline

From the above discussion it is clear that there remain many challenges when it comes to obtaining accurate absolute estimates of sO_2 *in vivo*. It is therefore important to note that even methods that can measure *differences* or changes in sO_2 would be of great interest clinically. One way this may be possible is by taking the difference in sO_2 estimates between vessels. If the errors in the sO_2 estimates due to spectral colouring are the same for each vessel, then the difference between their estimates will be accurate despite significant errors in their absolute sO_2 values. Estimates of the sO_2 difference could be used with artery-vein pairs (e.g. vennae comitantes), that typically have differences in sO_2 between 20% to 40% [28–30]. This information could be useful for surgical monitoring (locating arteries and veins before incision) or for estimating venous sO_2 when the vein is near a known artery (arteries typically have sO_2 between 95% and 100% under normal conditions). The latter can be used to assess the adequacy of tissue oxygenation [31].

Under what conditions will two vessels have equal spectral colouring biases? Assuming that noise and other experimental effects on image amplitude are negligible (i.e. the reconstruction is perfect), the spectral colouring bias of an sO_2 estimate acquired with the linear unmixing technique depends on how much the fluence in the voxel of interest varies with wavelength. This depends in turn on the absorption and scattering distributions within the tissue, and will therefore be sensitive to the locations, size, and optical properties of the vessels and other absorbers. As each tissue has a unique distribution of optical properties, it is difficult to formulate completely general rules for determining when the spectral colouring bias is identical for a pair of vessels. Nevertheless, some insights may be gathered by considering simpler tissue models. This paper aims to formulate some basic criteria for when the sO_2 difference may be accurate by considering tissue models consisting of two cylindrical vessels immersed in a two-layer skin model. An *in silico* study was performed to observe how the accuracy of the sO_2 difference changes for a pair of vessels placed in a variety of scenarios (e.g. when the distribution of absorbers and scatterers was varied by changing the size, location, and sO_2 of the vessels, as well as the properties of the background tissues).

Section 2 describes how the simulated images were generated. Section 3 describes each imaging trial and their results. To assess whether these criteria remain usefully accurate when considering more realistic images, they were tested in images of complex simulated tissue models featuring noise, reconstruction artefacts, complex distributions of vessels, and multiple skin layers (see Section 3.5). Conclusions are provided in Section 4.

2. Generating Simulated Images

This section describes each step involved in the generation of the simulated images used in this study.

2.1. Tissue Models

Tissue models were generated by immersing two 3D cylindrical vessels into a two-layer 3D tissue model. Each skin model consisted of an epidermis and dermis layer, where the thickness of the epidermis was set to a value between 0.1 and 0.3 mm. The vessel cross-sectional radii, sO_2, and location within the tissue model were varied within their normal physiological ranges for the study. The pair of vessels were aligned parallel to each other. This orientation was chosen to simplify the study by ensuring that the influence each vessel had on the other's fluence would not vary significantly across the length of each vessel for each simulation. The equations used to calculate the optical properties of each skin layer and the vessels at each excitation wavelength (784 nm, 796 nm, 808 nm, 820 nm) are presented in Table C1 in Appendix C. These wavelengths were chosen to ensure that the inversion was well-conditioned, and also because data was available for all skin layers in this range. The PA efficiency throughout each tissue was set to one.

2.2. Fluence Simulations

The fluence in each tissue model at each excitation wavelength was simulated with the Monte Carlo (MC) light model MCXLAB [32] on an NVIDIA Titan X Maxwell GPU (3072 CUDA cores, 12 GB of memory). The MC simulations were run with voxel sidelengths of 0.1 mm, and simulation volumes with dimensions of 40 x 40 x 40 voxels. A timestep of 10^{-11} s, and a total time of 10^{-9} s were used for each fluence simulation. A truncated collimated Gaussian beam with a waist radius of 20 voxels, with its centre placed on the centre of the top layer of the epidermis was used as the excitation source for the simulations. Photons exiting the domain were terminated. The initial pressure distributions were generated by voxel-wise multiplication of each fluence distribution with the corresponding optical absorption coefficients.

2.3. Image Noise

Note that in addition to the wavelength dependence of the fluence, image noise may also affect the accuracy of sO_2 estimates, as voxel amplitudes are affected in a way that is not constant with wavelength. The variance inherent in MC fluence simulations results in noise in the images generated from these fluence distributions. Although noise is present in real images, in this study the MC noise was reduced to a level at which it made little difference to the sO_2 estimates, in order to make it easier to study how variations in the properties of the vessels and tissue affected the accuracy of the sO_2 difference. Fluence simulations were therefore run with 10^9 photons giving a variance in sO_2 of $< 1\%$. (For more details see Appendix A.)

The effect that noise may have on the accuracy of the sO_2 estimates is sensitive to the condition number of the matrix containing the molar absorption coefficients [27]. Even in cases where there are low amounts of noise, wavelengths must be chosen so that condition number of the molar absorption coefficient matrix is small, and that changes in the initial pressure are strongly dependent on changes in sO_2. For this study, the noise associated with each image was minimised so that it had a negligible impact on sO_2 estimates acquired in each tissue model.

2.4. Image Processing

Because the sO_2 of the vessels may be different (and therefore have optical properties that vary differently with wavelength), the effect that the blood has on the spectral colouring bias should be minimised to provide more ideal conditions for producing an accurate sO_2 difference. For each tissue model, sO_2 estimates from each vessel were acquired from the most superficial voxel in the middle of each vessel. This voxel was chosen because its fluence is less dependent on the properties of the blood vessel it belongs to, as not all of the light propagating through it will have propagated through the vessel (as opposed to a voxel in the centre of a vessel, where all of the light travelling through it will have travelled through another portion of the vessel).

3. Simulation Trials

In this section, the results of a series of simulations showing how the sO_2 difference between two vessels changes in a variety of tissue environments/scenarios are presented.

3.1. Varying Vessel Depths

In many cases, the accuracy of the linear unmixing technique decreases as a vessel is positioned deeper within a tissue as even small variations in the tissue background's optical properties with wavelength can produce large differences in the fluence at depths exceeding a few millimeters [23]. How does the depth of each vessel in a pair affect the accuracy of their sO_2 difference? It is possible to gain some insight by considering an unrealistic case where a pair of vessels are immersed in an optically homogeneous tissue and the fluence can be modelled in 1D (i.e. Beer's law). In this case, the spectral colouring biases depend only on the optical properties of the tissue layer, and the depths of the vessels. Here, a pair of vessels

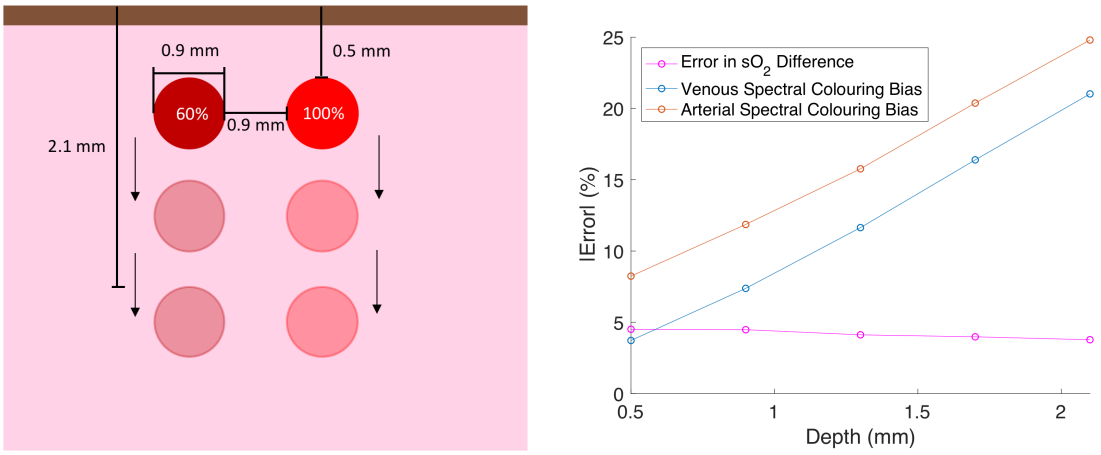

Figure 1: Left: Schematic of the tissue models used for studying how the accuracy of the sO_2 difference varies with the depths of the vessels. Right: Plot of the error in arterial and venous sO_2 and the intervascular difference in sO_2 for each simulation.

have equal spectral colouring biases provided they are at equal depths. In reality, the fluence depends on the optical properties of each vessel, as well as the optical properties elsewhere in the tissue. Vessels placed at the same depth may have significantly different spectral colouring biases due to presence of absorbers and scatterers dispersed throughout the tissue volume, or due to the properties of the vessels themselves. Therefore, it was of interest to see how depth might affect the accuracy of linear unmixing in a more realistic case. For our first trial, a series of simulations were conducted to find out whether the sO_2 difference can be accurate for two vessels at the same depth even in cases where the linear unmixing technique would produce inaccurate absolute sO_2 estimates for each vessel. This was tested for a variety of depths.

The sO_2 difference between an artery (100% sO_2) and a vein (60% sO_2) was estimated as both vessels were positioned at a series of depths within a simulated tissue volume. The vessels, each with a diameter of 0.9 mm, were separated by a lateral distance of 0.9 mm. The vessels were compared at depths of 0.5, 0.9, 1.3, 1.7 and 2.1mm. See Fig. 1. The epidermis was assigned a melanosome fraction of 3% and a thickness of 0.1 mm, the dermis was assigned a blood fraction of 7%, and an sO_2 of 100%. All of these values are typical for healthy human skin. The vessels shared the same depth for each simulation, as in the 1D case this condition would produce an accurate sO_2 difference and it was of interest to see whether this might still be the case when the fluence depends on the 3D distributions of absorbers and scatterers.

The results, Fig. 1, show that the sO_2 difference remains accurate with increasing vessel depth despite an increase in the spectral colouring bias for each vessel. For this tissue model, the spectral colouring biases are similar enough to produce accurate estimates of the sO_2 difference regardless of the magnitudes of the depths of the vessels in the tissue. For the rest of this work, vessels are placed at equal depths so that the effect that varying other tissue/vessels parameters may have on the sO_2 difference can be studied.

3.2. Varying Tissue Properties

Because melanin is highly absorbing and its optical properties vary with wavelength in the near infrared range, the accuracy of the linear unmixing technique depends heavily on the concentration of melanosomes in the epidermis. In many cases, the accuracy of an sO_2 estimate would be expected to decrease with an increase in the melanosome fraction in the epidermis as the fluence varies more strongly with wavelength. Although the presence of melanin can decrease the accuracy of absolute sO_2 estimates acquired with linear unmixing, the sO_2 difference between a pair of vessels may remain accurate if their

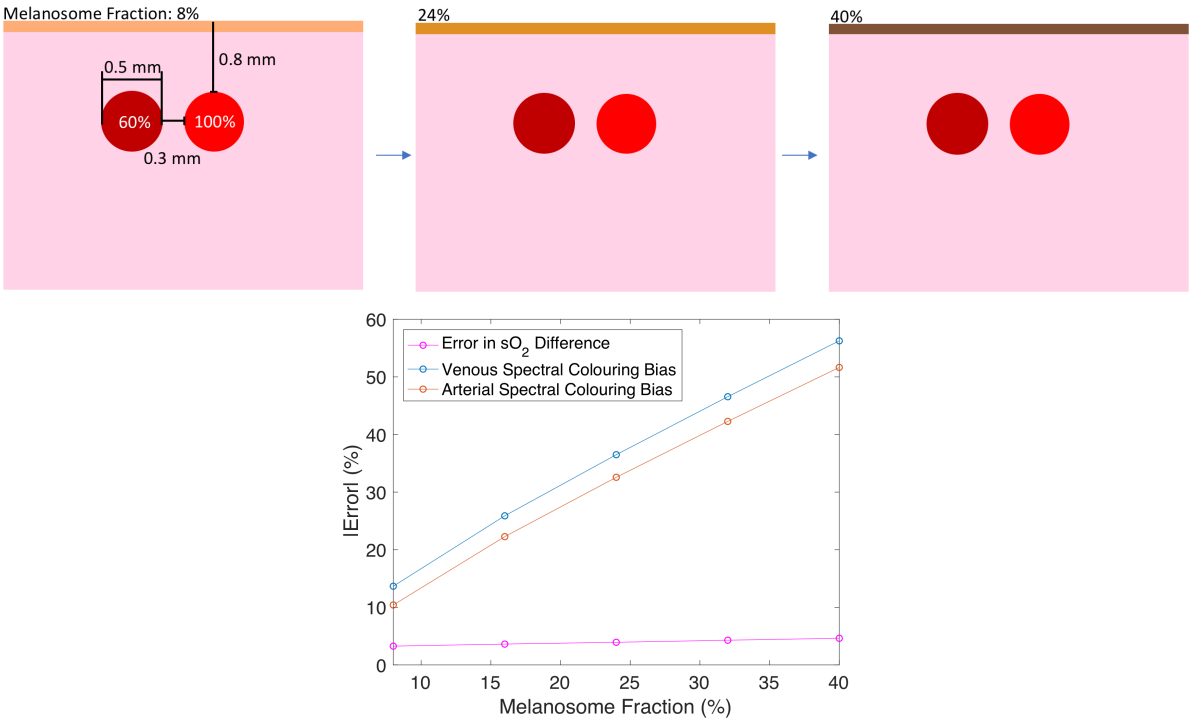

Figure 2: Top: Schematic of the tissue models used for studying how the accuracy of the sO_2 difference varies with increasing concentrations of melanin in the epidermis layer. Bottom: Plot of the error in arterial and venous sO_2 and the intervascular difference in sO_2 for each simulation.

spectral colouring biases are the same. Images were generated to observe how the accuracy of the sO_2 difference changes with an increase in the melanin within a tissue model.

The accuracy of the sO_2 difference in an artery (100% sO_2) and a vein (60% sO_2) at equal depths (0.8 mm) was calculated as the melanosome fraction of the epidermis was increased. The vessels were separated by a lateral distance of 0.3 mm as measured from their edges and were assigned diameters of 0.5 mm. The epidermis was assigned an initial melanosome fraction of 8% and a thickness of 0.3 mm, the dermis was assigned a blood fraction of 5%, and an sO_2 of 100%. The melanosome fraction was increased in four steps of 8%. The results in Fig. 2 show that the spectral colouring bias of both vessels increases as the melanosome fraction increases, and that the accuracy of the sO_2 difference remains roughly constant. All of the light emitted by the excitation source passes through the epidermis layer, which is distributed equally about the vessels. Thus, the effect that the melanosomes have on the fluence should be similar for both vessels, and thus, their sO_2 difference should be accurate.

3.3. Varying Vessel Properties

Because the fluence depends on the distribution of optical properties throughout the tissue, the spectral colouring bias of an sO_2 estimate depends on the optical properties of the blood in the vessels of interest, and on the size of the vessels. The effect that changing these parameters may have on the accuracy of the sO_2 difference was studied.

First, the accuracy of the sO_2 difference between an artery (100% sO_2) and a vein (68% sO_2) placed at equal depths (0.6 mm) was calculated as venous sO_2 was increased. The vessels were separated by a lateral distance of 0.3 mm as measured from their edges. The epidermis was assigned a melanosome fraction of 40% and a thickness of 0.3 mm, the dermis was assigned a blood fraction of 5%, and an sO_2 of 100%. The vein's sO_2 started at 68% and was increased by 8% for four additional steps. The

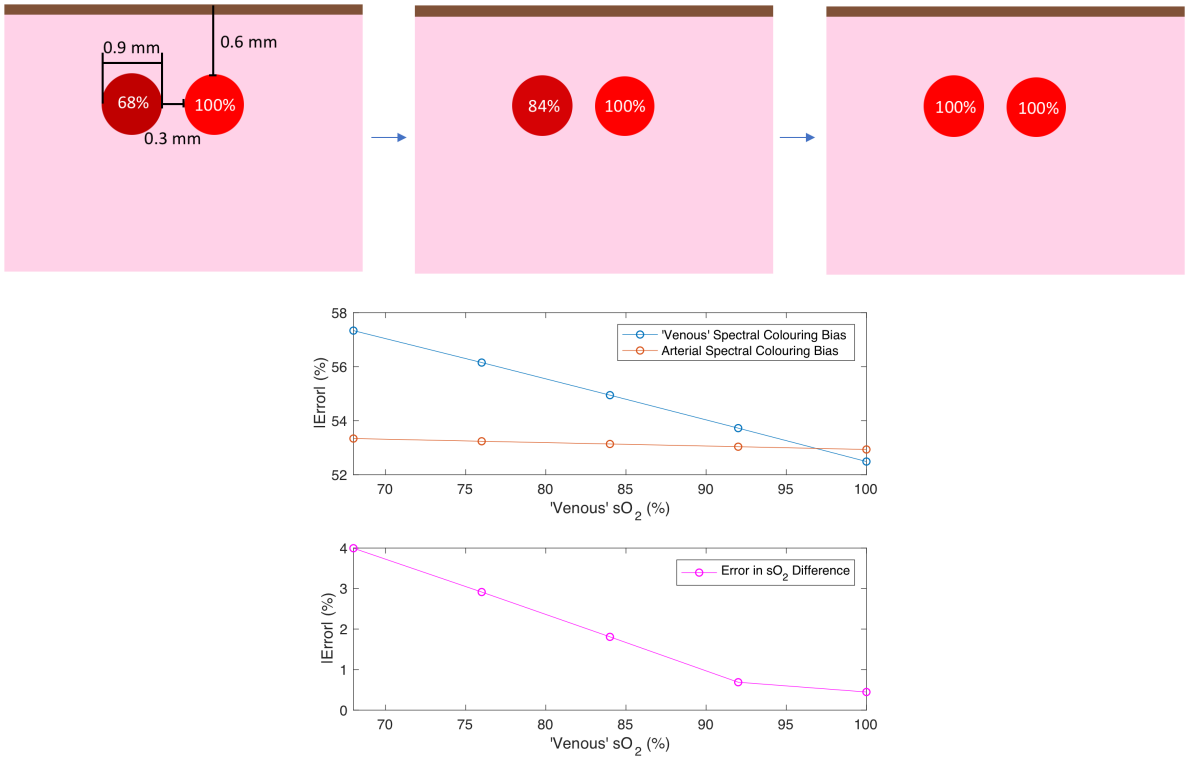

Figure 3: Top: Schematic of the tissue models used for studying how the accuracy of the sO_2 difference between an artery and vein pair varies with an increase in the venous sO_2. Bottom: Plot of the error in arterial and venous sO_2 and the intervascular difference in sO_2 for each simulation.

results are shown in Fig.3. The spectral colouring biases of each vessel became increasingly similar as the venous sO_2 approached 100%. The spectral colouring bias in a vessel is strongly determined by its optical properties. When the sO_2 values of the vessels are more similar, the wavelength dependence of their optical properties also become more similar, and hence, their spectral colouring biases also become more alike.

Another set of images were generated to study how the accuracy of the sO_2 difference changes with the size of the vessels. The accuracy of the sO_2 difference in an artery (100% sO_2) and a vein (60% sO_2) at equal depths (0.9 mm) was calculated as their radii were increased. The vessels were separated by a lateral distance of 0.3 mm as measured from their edges. The epidermis was assigned a melanosome fraction of 40% and a thickness of 0.3 mm, the dermis was assigned a blood fraction of 5%, and an sO_2 of 100%. The vessels had initial diameters of 0.5 mm, which were increased by 0.2 mm for eight steps. The results are shown in Fig. 4. The spectral colouring bias of the vessels are less equal as the size of the vessels increase, and thus the sO_2 difference become less accurate.

When a vessel is small, the effect that its optical properties have on its fluence is less significant compared to when it is larger. This is because if a vessel is large, more light that may end up propagating through the voxel of interest interacts with some other region of the vessel. Here, the value of sO_2 in the vessels were significantly different, and thus the optical properties of each vessel had a different wavelength dependence. One would therefore expect the wavelength dependence of the fluence in each vessel to become increasingly different as their size increases as their optical properties play a more significant role in determining the fluence.

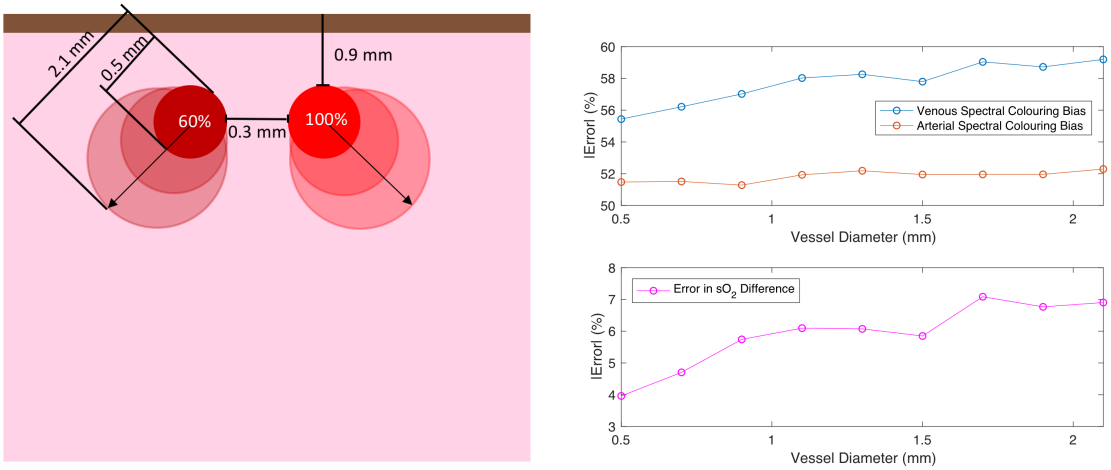

Figure 4: Top: Schematic of the tissue models used for studying how the accuracy of the sO_2 difference varies with an increase in the size of the vessels. Bottom: Plot of the error in arterial and venous sO_2 and the intervascular difference in sO_2 for each simulation.

3.4. Estimating the sO_2 Difference in the Presence of Additional Bodies

Real tissues have a complex distribution of absorbers and scatterers, and the influence that additional absorbers/scatterers (e.g. a vessel, or body of melanin) may have on the spectral colouring biases of a vessel pair must be taken into account to assess whether the difference in estimates may be accurate. This subsection presents the results of a set of simulations showing the effect that a neighbouring third vessel can have on the sO_2 difference between a vessel pair. For this test, a vessel pair (vein at 60% sO_2, and an artery at 100% sO_2) each with diameters of 0.5 mm were placed at equal depths (1 mm), and separated by a lateral distance of 0.9 mm. A third larger vessel with an sO_2 of 80% and a diameter of 0.9 mm was initially placed above the vein, and then translated across the tissue in steps of 0.1 mm for 16 steps. This will be referred to as the 'colouring' vessel, although of course all the vessels colour the fluence. In the initial orientation, the wavelength dependence of the optical properties of this colouring vessel strongly determine the wavelength dependence of the fluence in the vein beneath it, and to a lesser extent, the artery. This is because most of the light that may propagate into the vein will first propagate through the region just outside itself, and thus, whatever is in the vicinity of the vein may more strongly determine the fluence in it as opposed to other bodies in the tissue. The fluence in the artery is also affected by the colouring vessel, but not as significantly, as a large portion (but certainly not all) of the light that is likely to propagate through the artery will not interact with the colouring vessel as it is further away from the artery. The epidermis was assigned a melanosome fraction of 40% and a thickness of 0.3 mm, the dermis was assigned a blood fraction of 5%, and an sO_2 of 100%.

The sO_2 difference is accurate when the colouring vessel is near the midpoint between the vessels, where the influence that the colouring vessel has on each vessel is similar. The difference is most accurate when the colouring vessel is slightly offset from the midpoint. At first this may seem counterintuitive, as the third vessel is equidistant to the artery and vein and thus should have a similar effect on the fluence in both, resulting in the most accurate sO_2 difference. However, the fluence in the artery and vein also depends on their optical properties. As we've seen in previous trials (Section 3.3), if vessels have different sO_2s, they can have different spectral colouring biases even if they are at the same depth. To offset this difference in the spectral colouring biases, the third vessel must affect the fluence in one vessel more than the other, and thus the most accurate sO_2 difference should occur when the colouring vessel is closer to one vessel than the other. Fig. B1 in Appendix B confirms this, as it shows the results of the same test when the sO_2 of the artery and vein are identical. Here, the blood in the artery and vein affects their fluence in the same way, and we find that the difference is most accurate when the third vessel is

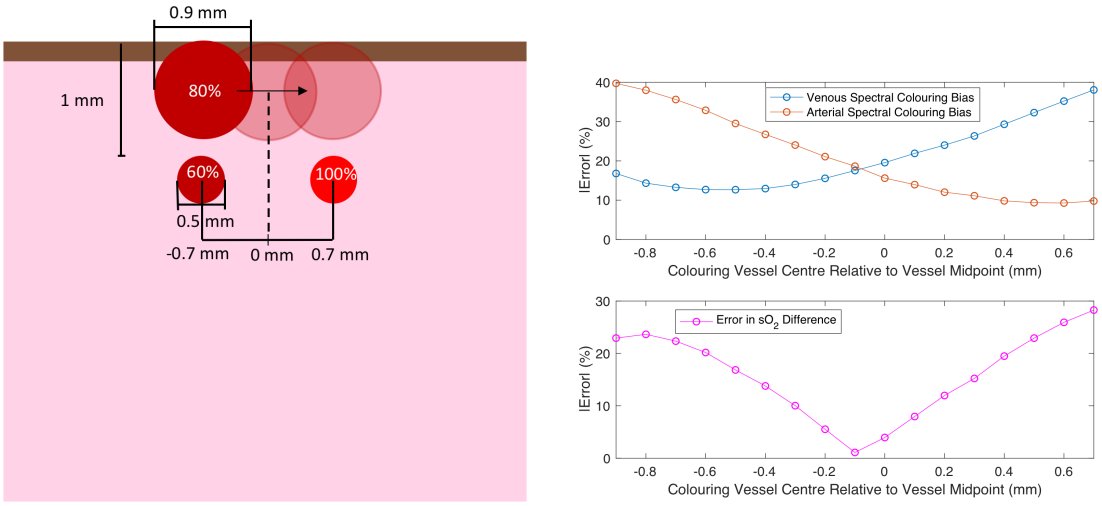

Figure 5: Left: Schematic of the tissue models used for studying how the accuracy of the sO_2 difference between a pair of vessels varies as a third 'colouring vessel' is placed at various distances from each vessel. Right: Plot of the error in arterial and venous sO_2 and the intervascular difference in sO_2 for each simulation.

exactly at the midpoint.

In this example, despite the fact that the vessels are at the same depth, the sO_2 difference is not accurate. This set of simulations shows that the effect of all the absorbers/scatterers present in the tissue must be considered when determining whether the sO_2 difference may be accurate.

3.5. Criteria for Estimating Accurate sO_2 Differences and Validation in Complex Tissue Models

In this work, simulations using idealised tissue models were used to formulate criteria for when the sO_2 difference between a pair of vessels may be accurately determined from PA spectra when the fluence difference is ignored. *In vivo* tissues feature a much more complex distribution of absorbers and scatterers, and the image amplitude depends on experimental factors such as noise and reconstruction artefacts, so any criteria that are drawn from these simulations may fail in scenarios where the influence of additional absorbers/scatterers or experimental factors may have to be considered. Based on the results of these trials, the sO_2 difference appears to be more accurate when the following criteria are met:

(i) The vessels are at the same depth,

(ii) the vessels have similar sO_2 values,

(iii) the vessels are small.

To test the accuracy of these criteria using more complex tissue models, images were simulated for three additional tissue models, and the sO_2 difference between two vessels within each tissue model satisfying these criteria was estimated. The acoustic propagation, detection of pressure time series with a planar sensor array, and the reconstruction of the images were simulated at each excitation wavelength using k-Wave [33] to produce images with noise and reconstruction artefacts. Tissue models were generated by immersing 3D vessel models acquired from CT images of human lungs into 3D, three-layer skin models [34, 35]. Images/models were generated following the procedure in [15]. The results are shown in Fig. 6. The accuracy of the sO_2 difference in all three tissue models is larger than the accuracy of the absolute estimates of sO_2. These results indicate that even in more realistic scenarios, the criteria derived in this paper may indicate scenarios where the sO_2 difference is accurate. However, as they are based on simple tissue models, these criteria should be used cautiously, for example as a starting point for further, more detailed, investigations of any specific target geometry.

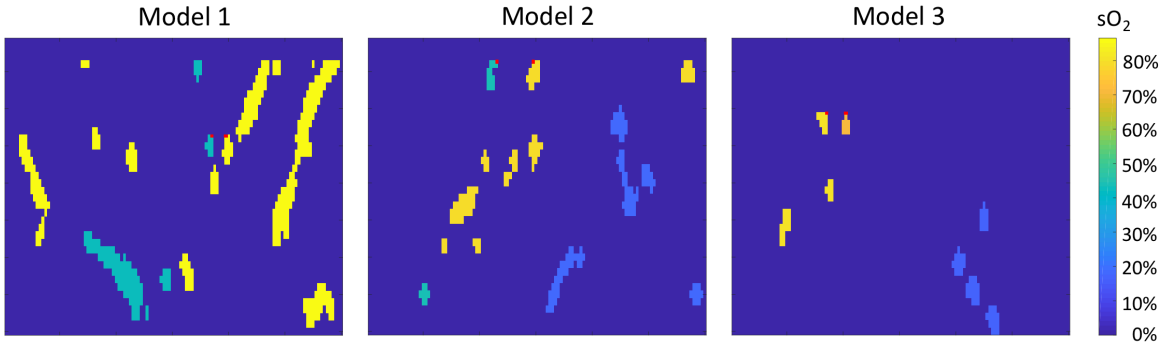

Tissue Model	Epidermis Melanosome Fraction	Dermis Blood Fraction	Dermis sO_2	sO_2 Difference	|Error|
1	38.0%	2.6%	60.4%	38.7%	4.6%
2	13.3%	7.0%	68.4%	29.3%	6.4%
3	25.6%	4.01%	66.4%	8.0%	1.2%

Figure 6: Top: 2D slices of the 3D sO_2 distribution of three complex tissue models used for assessing whether the sO_2 difference can be accurate in more realistic tissue models. Voxels from which the difference in sO_2 was estimated are shown in red. Bottom: Table showing the properties of each tissue model and the results of the test.

4. Conclusions

Because of spectral colouring, linear spectroscopic unmixing can rarely be used to acquire accurate estimates of sO_2 in tissue from uncorrected photoacoustic spectra. However, in cases where the effects of spectral colouring are the same for a pair of vessels, the difference in sO_2 estimates may be accurate. By studying simple tissue models consisting of a pair of vessels immersed in a two-layer skin model, the spectral colouring bias was found more likely to be equal when the vessels were at the same depth, smaller, and had similar oxygenation levels. The sO_2 difference between arteries and veins can be anywhere between 20% - 40% under normal healthy conditions whereas the sO_2 difference between veins can take values between 0%-15% given that the typical range for venous sO_2 is between 60%-75% [29, 30]. To ensure that the characterisation of any artery/vein pairs is correct, estimates must be accurate within 5% (where all estimates between 15%-20% should be considered inconclusive). The results of our tests in simplified tissue models have shown that when these conditions are satisfied, it is possible to achieve estimates within this range of accuracy.

In real tissue, the spectral colouring depends on the unique distribution of absorbers and scatterers in a given tissue. Therefore, care must be exercised when using these criteria in more realistic settings. However, accurate sO_2 differences were acquired from simulated images of more realistic tissue models, suggesting that these criteria may still be useful as a starting point in more realistic imaging scenarios.

Acknowledgements

The authors would like to thank Paul Beard and UCL's Photoacoustic Imaging Group for useful discussions. CB acknowledges funding from the BBSRC London Interdisciplinary Doctoral Programme, LIDo.

References

[1] Beard P 2011 *Interface Focus* **1** 602–631
[2] Cox B T, Laufer J G, Beard P C and Arridge S R 2012 *Journal of Biomedical Optics* **17** 061202
[3] Hussain A, Petersen W, Staley J, Hondebrink E and Steenbergen W 2016 *Optics Letters* **41** 1720–1723
[4] Fonseca M, Malone E, Lucka F, Ellwood R, An L, Arridge S, Beard P and Cox B 2017 *Photons Plus Ultrasound: Imaging and Sensing 2017* vol 10064 (International Society for Optics and Photonics) p 1006415

[5] Cox B T, Arridge S R, Köstli K P and Beard P C 2006 *Applied Optics* **45** 1866–1875
[6] Buchmann J, Kaplan B, Powell S, Prohaska S and Laufer J 2020 *Photoacoustics* 100157
[7] Buchmann J, Kaplan B A, Powell S, Prohaska S and Laufer J 2019 *Journal of Biomedical Optics* **24** 066001
[8] Arridge S, Maass P, Öktem O and Schönlieb C B 2019 *Acta Numerica* **28** 1–174
[9] Gröhl J, Kirchner T, Adler T and Maier-Hein L 2019 *arXiv preprint arXiv:1902.05839*
[10] Yang C and Gao F 2019 *International Conference on Medical Image Computing and Computer-Assisted Intervention* (Springer) pp 246–254
[11] Luke G P, Hoffer-Hawlik K, Van Namen A C and Shang R 2019 *arXiv preprint arXiv:1911.01935*
[12] Chen T, Lu T, Song S, Miao S, Gao F and Li J 2020 *Photons Plus Ultrasound: Imaging and Sensing 2020* vol 11240 (International Society for Optics and Photonics) p 112403V
[13] Yang C, Lan H, Zhong H and Gao F 2019 *2019 IEEE 16th International Symposium on Biomedical Imaging (ISBI 2019)* (IEEE) pp 741–744
[14] Cai C, Deng K, Ma C and Luo J 2018 *Optics Letters* **43** 2752–2755
[15] Bench C, Hauptmann A and Cox B 2020 *arXiv preprint arXiv:2005.01089*
[16] Xia J, Danielli A, Liu Y, Wang L, Maslov K and Wang L V 2013 *Optics Letters* **38** 2800–2803
[17] Carome E, Clark N and Moeller C 1964 *Applied Physics Letters* **4** 95–97
[18] Cross F, Al-Dhahir R, Dyer P and MacRobert A 1987 *Applied Physics Letters* **50** 1019–1021
[19] Cross F, Al-Dhahir R and Dyer P 1988 *Journal of Applied Physics* **64** 2194–2201
[20] Guo Z, Hu S and Wang L V 2010 *Optics Letters* **35** 2067–2069
[21] Deng Z and Li C 2016 *Journal of Biomedical Optics* **21** 061009
[22] Kim S, Chen Y S, Luke G P and Emelianov S Y 2011 *Biomedical Optics Express* **2** 2540–2550
[23] Li M, Tang Y and Yao J 2018 *Photoacoustics* **10** 65–73
[24] Yao J, Maslov K I, Zhang Y, Xia Y and Wang L V 2011 *Journal of Biomedical Optics* **16** 076003
[25] Stein E W, Maslov K I and Wang L V 2009 *Journal of Biomedical Optics* **14** 020502
[26] Li Q, Yu T, Li L, Chai X and Zhou C 2016 *Optics in Health Care and Biomedical Optics VII* vol 10024 (International Society for Optics and Photonics) p 100242E
[27] Hochuli R, An L, Beard P C and Cox B T 2019 *Journal of Biomedical Optics* **24** 121914
[28] Gray H 1918 *Anatomy of the Human Body* (Philadelphia: Lea and Febiger)
[29] Rivers E P, Ander D S and Powell D 2001 *Current opinion in critical care* **7** 204–211
[30] Lindholm L, Hansdottir V, Lundqvist M and Jeppsson A 2002 *Perfusion* **17** 133–139
[31] Marx G and Reinhart K 2006 *Current opinion in critical care* **12** 263–268
[32] Fang Q Monte Carlo eXtreme (MCX) - GPU-accelerated photon transport simulator `https://github.com/fangq/mcx` URL `https://github.com/fangq/mcx`
[33] Treeby B E and Cox B T 2010 *Journal of Biomedical Optics* **15** 021314
[34] Hauptmann A, Lucka F, Betcke M, Huynh N, Adler J, Cox B, Beard P, Ourselin S and Arridge S 2018 *IEEE transactions on medical imaging* **37** 1382–1393
[35] Group V Public Lung Image Database `http://www.via.cornell.edu/lungdb.html` URL `http://www.via.cornell.edu/lungdb.html`
[36] Jacques S L Skin optics summary `https://omlc.org/news/jan98/skinoptics.html` accessed: 2019-03-21 URL `https://omlc.org/news/jan98/skinoptics.html`
[37] Jacques S Optical absorption of melanin `https://omlc.org/spectra/melanin/` accessed: 2019-03-21 URL `https://omlc.org/spectra/melanin/`
[38] Jacques S L 2013 *Physics in Medicine & Biology* **58** R37
[39] Ding H, Lu J Q, Wooden W A, Kragel P J and Hu X H 2006 *Physics in Medicine & Biology* **51** 1479
[40] Bashkatov A N, Genina E A and Tuchin V V 2011 *Journal of Innovative Optical Health Sciences* **4** 9–38
[41] Tuchin V V and Tuchin V 2007 *Tissue optics: Light Scattering Methods and Instruments for Medical Diagnosis* (SPIE Press Bellingham)
[42] Yudovsky D and Pilon L 2011 *Journal of Biophotonics* **4** 305–314
[43] Lazareva E N and Tuchin V V 2018 *Journal of Biomedical Photonics & Engineering* **4**
[44] Bashkatov A, Genina E, Kochubey V and Tuchin V 2005 *Journal of Physics D: Applied Physics* **38** 2543
[45] Faber D J, Aalders M C, Mik E G, Hooper B A, van Gemert M J and van Leeuwen T G 2004 *Physical Review Letters* **93** 028102

Appendix A. Noise Test

For each tissue model, a noise test was conducted to ensure that the variance in the fluence estimates produced a variance of $< 1\%$ for each sO_2 estimate.

For a given tissue model, the fluence was run at each excitation wavelength 20 times. The most superficial voxel in the middle of each vessel was used for the noise test. The standard deviation in the

sO_2 estimate in one voxel was calculated using,

$$\sigma_{sO_2} = sO_2 \sqrt{\left(\frac{\partial sO_2}{\partial p_0(\lambda_1)}\sigma_{p_0(\lambda_1)}\right)^2 + \left(\frac{\partial sO_2}{\partial p_0(\lambda_2)}\sigma_{p_0(\lambda_2)}\right)^2 + \left(\frac{\partial sO_2}{\partial p_0(\lambda_3)}\sigma_{p_0(\lambda_3)}\right)^2 + \left(\frac{\partial sO_2}{\partial p_0(\lambda_4)}\sigma_{p_0(\lambda_4)}\right)^2},$$

(assuming that the initial pressures are uncorrelated) where the values for $\sigma_{p_0(\lambda)}$ were calculated by taking the standard deviation of the initial pressure values in the voxel of interest over all 20 runs [27]. sO_2 was calculated using Eqs. (4) and (3).

Appendix B. Identical sO_2 Colouring Vessel Test

Figure B1 shows the results of performing the same colouring vessel test mentioned in Section 3.4, but with the vessels in the pair set to have equal sO_2s.

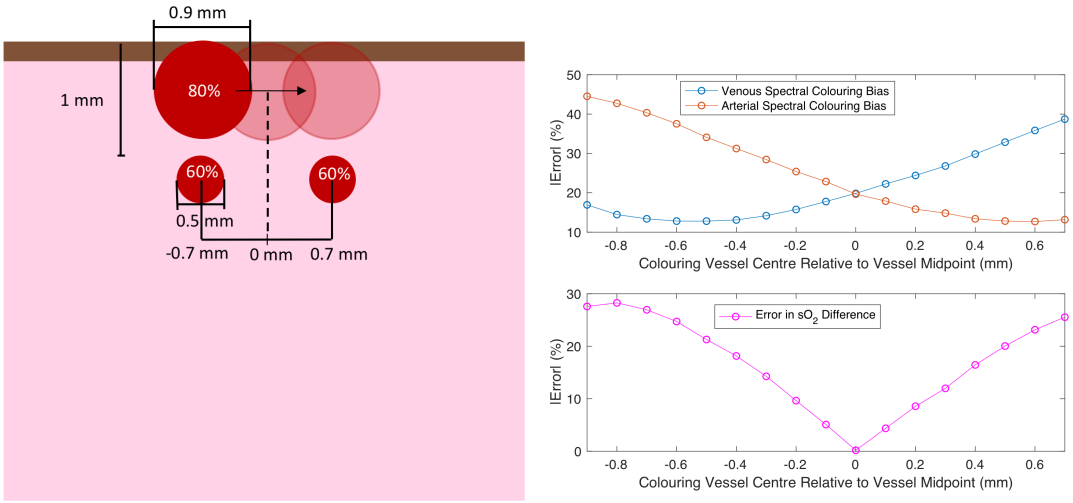

Figure B1: Left: Schematic of the tissue models used for studying how the accuracy of the sO_2 difference between a pair of vessels varies as a third 'colouring vessel' is placed at various distances from each vessel, and where each vessel in the pair has the same sO_2. Right: Plot of the error in arterial and venous sO_2 and the intervascular difference in sO_2 for each simulation.

Appendix C. Optical Properties of Skin Layers

The refractive index, anisotropy factor, optical absorption coefficient, and the optical scattering coefficient of each tissue/chromophore type are required to run a fluence simulation for a tissue model. Relevant values/expressions for calculating these properties are provided in Table C1.

Table C1: Skin optical properties (λ is given in nm).

Tissue	Parameter	Value	Ref.
Epidermis	Optical absorption (cm^{-1})	$\mu_{ae} = (C_M 6.6(\lambda^{-3.33})(10^{11})) + (1 - C_M)(0.244 + 85.3(\exp(-\frac{\lambda - 154}{66.2})))$	[36]
	Melanosome fraction C_M	6% for Caucasian skin, 40% for pigmented skin	[37]
	Reduced scattering (cm^{-1})	$\mu_s' = 68.7(\frac{\lambda}{500})^{-1.16}$	[38]
	Refractive index	1.42 - 1.44 (700 nm - 900 nm)	[39]
	Anisotropy	0.95 - 0.8 (700 nm - 1500 nm)	[40, 41]
	Thickness	0.1 mm	
Dermis	Optical absorption (cm^{-1})	$\mu_{ad} = C_B \mu_{ab} + (1 - C_B)(0.244 + 85.3(\exp(-\frac{\lambda - 154}{66.2})))$	[36]
	Blood volume fraction C_B	0.2% - 7%	[42]
	Reduced scattering (cm^{-1})	$\mu_s' = 45.3(\frac{\lambda}{500})^{-1.292}$	[38]
	Refractive index	$n = A + \frac{B}{\lambda^2} + \frac{C}{\lambda^4}$, where $A = 1.3696$, $B = 3.9168\text{x}10^3$, $C = 2.5588\text{x}10^3$	[39]
	Anisotropy	0.95 - 0.8 (700 nm - 1500 nm)	[40, 41]
	sO_2	40% - 100%	[42]
Blood	Optical absorption (cm^{-1})	$\mu_{ab} = C_{Hb}\alpha_{Hb} + C_{HbO_2}\alpha_{HbO_2}$	[36]
	Reduced scattering (cm^{-1})	$22(\frac{\lambda}{500})^{-0.66}$	[38]
	Refractive index	1.36 (680 nm - 930 nm)	[43]
	Anisotropy	0.994 (Roughly constant for variant wavelength and sO_2)	[44, 45]